Regularizing method for the determination of the backscatter cross section in lidar data

Yanfei Wang,[1,*] Jianzhong Zhang,[2] Andreas Roncat,[3] Claudia Künzer,[2] and Wolfgang Wagner[3]

[1]*Key Laboratory of Petroleum Geophysics, Institute of Geology and Geophysics, Chinese Academy of Sciences, PO Box 9825, Beijing 100029, China*

[2]*German Remote Sensing Data Center (DFD), German Aerospace Center (DLR), Oberpfaffenhofen, PO Box 1116, D-82230 Wessling, Germany*

[3]*Christian Doppler Laboratory for Spatial Data from Laser Scanning and Remote Sensing, Vienna University of Technology, Gusshausstrasse 27-29, 1040 Vienna, Austria*

[*]*Corresponding author: yfwang_ucf@yahoo.com*

Received November 6, 2008; revised February 15, 2009; accepted February 18, 2009; posted February 20, 2009 (Doc. ID 103764); published April 1, 2009

The retrieval of the backscatter cross section in lidar data is of great interest in remote sensing. For the numerical calculation of the backscatter cross section, a deconvolution has to be performed; its determination is therefore an ill-posed problem. Most of the common techniques, such as the well-known method of Gaussian decomposition, make implicit assumptions on both the emitted laser pulse and the scatterers. It is well understood that a land surface is quite complicated, and in many cases it cannot be composed of pure Gaussian function combinations. Therefore the assumption of Gaussian decomposition of waveforms may be invalid sometimes. In such cases an inversion method might be a natural choice. We propose a regularizing method with *a posteriori* choice of the regularizing parameter for solving the problem. The proposed method can alleviate difficulties in numerical computation and can suppress the propagation of noise. Numerical evidence is given of the success of the approach presented for recovering the backscatter cross section in lidar data.

OCIS codes: 100.1830, 140.3538, 280.3640, 100.3190.

1. INTRODUCTION

Airborne laser scanning (ALS) is an active remote sensing technique that is also often referred to as lidar or laser radar. As a result of the increasing availability of sensors, ALS has been receiving increasing attention in recent years (e.g., see [1–4]). In ALS a laser emits short infrared pulses toward the Earth's surface, and a photodiode records the backscattered echo. With each scan, measurements are taken of the round trip time of the laser pulse, the received echo power, and the beam angle in the locator's coordinate system. The round-trip time of the laser pulse allows calculating the range (distance) between the laser scanner and the object that generated the backscattered echo. Thereby, information about the geometric structure of the Earth's surface is obtained. The received power provides information about the scattering properties of the targets that can be exploited for object classification and for modeling of the scattering properties.

The latest generation of ALS systems not only records a discrete number of echoes but also digitizes the whole waveform of the reference pulse and the backscattered echoes. In this way, besides the range, further echo parameters can be determined. The retrieval of the backscatter cross section is of great interest in full-waveform ALS. Since it is calculated by deconvolution, its determination is an ill-posed problem in a general sense. So far, most of the developed methods are based on the implicit assumption of Gaussian scatterers, i.e., the cross section profile in the time domain can be represented by a sum of Gaussian functions, whereby each echo represents a cluster of scatterers situated too closely to be resolved by the range resolution of the ALS system (see [3]). However, given the complex form and reflectivity properties of natural and man-made objects and considering intensity variations of the laser beam over its footprint, one has to expect that this assumption is, in a strict sense, often not correct.

On the other hand, determination of the scattering cross section from the observed waveform is an inherently ill-posed problem, i.e., we cannot hope to obtain a unique solution unless we impose additional constraints based on *a priori* knowledge or assumptions (see [5]). However, the incorporation of constraints is not a trivial task; they may come from several sources, historically, empirically, or quantitatively (see [6]). For the backscatter cross section in lidar data, quantitative information can be gained by assuming the scaled backscatter cross section is upper bounded. More specifically, we present in Subsection 3.B a mathematical model that incorporates constraints to the backscatter cross section, and we solve a L_2 norm problem with Sobolev norm function as a constraint. This formulation solves many types of ill-posed inverse problems, and it is a basis for the inversion theory (see [7]).

The rest of the paper is organized as follows. In Section 2, we recall the modeling of laser scanning signals and the derivation of the convolution system. In Section 3, we propose a regularization method for determination of the cross section; issues of deconvolution and ill-posed nature of the inverse problem, regularization model, and regularization techniques are discussed in Subsections 3.A–3.D,

respectively. In Section 4, we present numerical results to confirm our assertion. Some concluding remarks are given in Section 5. Finally, we supply appendices for some computational procedures.

Throughout the paper we use the following notation: ":=" denotes "defined as;" "$\mathbf{x}$" denotes the discretization of a function x, "min" denotes "minimizing" a functional, "A^*" denotes the adjoint of an operator A, "A^T" denotes the transpose of a matrix A, and "s.t." denotes "subject to."

2. MODELING OF LASER SCANNING SIGNALS

ALS utilizes a measurement principle strongly related to radar remote sensing. The fundamental relation to explain the signal strength in both techniques is the radar equation (see [3]):

$$P_r(t) = \frac{D_r^2}{4\pi R^4 \beta_t^2} P_t\left(t - \frac{2R}{v_g}\right)\sigma, \tag{1}$$

where t is the time, R is the range, D_r is the aperture diameter of the receiver optics, β_t is the transmitter beam width, P_t is the transmitted power of the laser, and σ denotes the scattering cross section. The time delay is equal to $t' = 2R/v_g$, where v_g is the group velocity of the laser pulse in the atmosphere.

Taking the occurrence of multiple scatterers into account and considering the receiver impulse response $\Gamma(t)$ of the system's receiver, for N distinct targets within the travel path of the laser pulse, we get [3]

$$P_r(t) = \sum_{i=1}^{N} \frac{D_r^2}{4\pi R_i^4 \beta_t^2} P_t(t) \star \sigma_i'(t) \star \Gamma(t), \tag{2}$$

where $\star$ denotes the convolution operator, and $\sigma_i'(t)$ is the differential backscatter cross section at the mean range position R_i. Since convolution is commutative, we can set $P_t(t)\star\sigma_i'(t)\star\Gamma(t) = P_t(t)\star\Gamma(t)\star\sigma_i'(t) = f(t)\star\sigma_i'(t)$, i.e., it is possible to combine both the transmitter and the receiver characteristics into a single term $f(t)$. This term is referred to as the *system waveform* of the laser scanner (see [3]). For simplifying notation, we define $g(t) = \sum_{i=1}^{N} R_i^{-4}\sigma_i'(t)$ and $h(t) = 4\pi\beta_t^2/D_r^2 P_r(t)$. Thus, we are able to write our problem in the form

$$h(t) = (f \star g)(t), \tag{3}$$

where h is the incoming signal recorded by the receiver, f denotes a mapping that specifies the kernel function or point-spread function, and g is the unknown cross section.

3. REGULARIZATION METHOD FOR DETERMINATION OF THE CROSS SECTION

A. Deconvolution

The received pulse consists of an effective wave $h_{eff}(t)$ and an additive noise $n(t)$:

$$h(t) = h_{eff}(t) + n(t).$$

Therefore, it is quite important to stably retrieve the cross section from Eq. (3) and suppress the perturbation simultaneously. We may write $h_{eff}(t)$ in the form

$$f \star g_{eff} = h_{eff}, \tag{4}$$

where g_{eff} denotes the actual backscatter cross section.

Now the problem is how to deconvolve the convolution Eq. (3) to get the approximation to the actual cross section g_{eff}. If we can identify an operator that is the inverse of $f(t)$, then $g_{eff}(t)$ can be obtained directly. Though this is perfect in theory, this approach may not work well in practice. Numerically, the inverse of $f(t)$ is hard to obtain.

Let us rewrite problem (3) into the abstract operator form,

$$Fg = h, \tag{5}$$

where $F: G \to H$ is a mapping and $g \in G$, $h \in H$. Both G and H can be considered to be Hilbert spaces. Because of the intrinsic ill-posedness of the problem, a large jump occurs for $F^{-1}n$, so to $F^{-1}h$. For noninvertible operator K, a least-squares error method may be applied that solves a residual minimization problem:

$$\|Fg - h\|^2 \to \min. \tag{6}$$

However the solution

$$\tilde{g} = \sum_k \frac{(h, v_k)}{\sigma_k} u_k = \sum_k \left[\frac{(h_{eff}, v_k)}{\sigma_k} u_k + \frac{(n, v_k)}{\sigma_k} u_k \right]$$

is unstable for ill-posed problems (a poor approximation to g_{eff}), since $(n, v_k)/\sigma_k$ may be astonishingly large for random noise n [8], where $\{\sigma_k; u_k, v_k\}$ is the singular system of F.

B. Regularization

It is natural to require error between the observed and the true land-surface signal to be as small as possible, i.e., the energy of noise to be minimal,

$$\|n\| \to \min.$$

Here $\|\cdot\|$ is the norm in any form. However, due to the ill-posed nature of deconvolution, the above problem is unstable. Therefore introducing a regularization technique is necessary.

For effective inversion of the ill-posed linear operator equation, we must impose an *a priori* constraint on the interested parameters. This leads to solving a constrained least-squares error problem,

$$\min J[g] := \|Fg - h\|^2, \tag{7}$$

$$\text{s.t. } c(g) \leqslant \Delta, \tag{8}$$

where $c(g)$ is the constraint to the solution g, and Δ is a constant that specifies the upper bound of $c(g)$. Usually, $c(g)$ is chosen as the norm of g with different scale. If the parameter g comes from a smooth function, then $c(g)$ can be chosen as a smooth function; otherwise, $c(g)$ can be nonsmooth. A generically used constraint is the smoothness. It assumes that physical properties in a neighborhood of space or in an interval of time present some coherence and generally do not change abruptly. Practically, we can always find regularities of a physical phenomenon with respect to certain properties over a short period of time. The smoothness *a priori* has been one of the most popular assumptions in applications.

The general framework for fulfilling the above requirement is the so-called regularization. We consider a canonical regularization model (see [7])

$$\min\|Fg-h\|_{L_2}^2+\nu\Gamma(g), \tag{9}$$

where $\Gamma(\cdot)$ is a function whose role is to give some penalization to the unknown cross section g, and $\nu>0$ is the regularization parameter. Here, the L_2 space is defined as the set of functions that is square-integrable, i.e., $L_2(\Omega):=\{g(t):\int_\Omega|g(t)|^2\mathrm{d}t<\infty\}$.

C. Choosing the Weighting Factor Matrix

To ensure the convexity of the optimized problem (9), it is necessary to choose the appropriate regularization parameter ν and the penalty function $\Gamma(g)$. Usually, $\Gamma(g)$ is chosen as a quadratic form $\Gamma(g)=(Lg,g)$. There are several ways for choosing the matrix L. A simple way is choosing the L as the identity, i.e., the weight imposed on each element is identical. However it is reported in [6] and [9] that the choice of $\Gamma(g)$ as a Sobolev norm function of the form $\Gamma[g]=\|g\|_{W^{1,2}}^2$ has a better conditioning state than others. Here the Sobolev $W^{1,2}$ space is defined as the set of functions that is continuous and differentiable with the bounded norms of itself and its generalized derivatives in L_2, i.e., $W^{1,2}(\Omega):=\{g(t):g(t)\in C(\Omega),g(t)\in L_2(\Omega),\mathrm{d}g/\mathrm{d}t\in L_2(\Omega),\int_\Omega(g^2+\Sigma_{i=1}^n(\mathrm{d}g/\mathrm{d}t_i)^2)\mathrm{d}t_1\mathrm{d}t_2\ldots\mathrm{d}t_n<\infty\}$, where $C(\Omega)$ denotes the continuous space. The inner product of two functions $g_1(\tau)$ and $g_2(\tau)$ in $W^{1,2}$ space is defined by

$$[g_1(\tau),g_2(\tau)]_{W^{1,2}}:=\int_\Omega\left[g_1(\tau)g_2(\tau)+\sum_{i,j=1}^n\frac{\partial g_1}{\partial\tau_i}\frac{\partial g_2}{\partial\tau_j}\right]\mathrm{d}\tau_1\mathrm{d}\tau_2\ldots\mathrm{d}\tau_n, \tag{10}$$

where Ω is the assigned interval of the definition.

Assume that the variation of $g(\tau)$ is flat near the boundary of the integral interval Ω. In this case, the derivatives of g are zero at the boundary of Ω. Let s_t be the step size of the grids in Ω, then after discretization of $\Gamma[g]$, L is a tridiagonal matrix in the form

$$L=\begin{bmatrix}1+\frac{1}{s_t^2} & -\frac{1}{s_t^2} & 0 & \cdots & 0\\ -\frac{1}{s_t^2} & 1+\frac{2}{s_t^2} & -\frac{1}{s_t^2} & \cdots & 0\\ \vdots & \ddots & \ddots & \ddots & \vdots\\ 0 & \cdots & -\frac{1}{s_t^2} & 1+\frac{2}{s_t^2} & -\frac{1}{s_t^2}\\ 0 & \cdots & 0 & -\frac{1}{s_t^2} & 1+\frac{1}{s_t^2}\end{bmatrix}.$$

In our numerical experiment, the step size s_t is 1.

D. Choosing the Regularization Parameter

Choosing the regularization parameter ν is also an important issue. *A priori* choice of the parameter ν requires $0<\nu<1$. However the *a priori* choice of the parameter does not reflect the degree of approximation that may lead to either overestimation or underestimation of the regularizer. It is well known that the *a posteriori* parameter choice rule can yield better recoveries. We adopt a widely used discrepancy principle (see [7]).

In fact, the optimal parameter ν^* is a root of the nonlinear function

$$\Psi(\nu)=\|Fg_\nu-h\|^2-\delta^2, \tag{11}$$

where δ is the error level to specify the approximate degree of the observation relative to the true noiseless data. Noting $\Psi(\nu)$ is differentiable, fast algorithms for solving the optimal parameter ν^* can be implemented. In this paper we will use the cubic convergent algorithm developed in [10]:

$$\nu_{k+1}=\nu_k-\frac{2\Psi(\nu_k)}{\Psi'(\nu_k)+[\Psi'(\nu_k)^2-2\Psi(2\nu_k)\Psi''(\nu_k)]^{1/2}}. \tag{12}$$

In the above cubic convergent algorithm, the functions $\Psi'(\nu)$ and $\Psi''(\nu)$ have the explicit expressions

$$\Psi'(\nu)=-\nu\beta'(\nu),$$

$$\Psi''(\nu)=-\beta'(\nu)-2\nu\left[\left\|L^{1/2}\frac{\mathrm{d}g_\nu}{\mathrm{d}\nu}\right\|^2+\left(Lg_\nu,\frac{\mathrm{d}^2g_\nu}{\mathrm{d}\nu^2}\right)\right],$$

where $\beta(\nu)=\|L^{1/2}g_\nu\|^2$, $\beta'(\nu)=2(L\mathrm{d}g_\nu/\mathrm{d}\nu,g_\nu)$, and g_ν, $\mathrm{d}g_\nu/\mathrm{d}\nu$, and $\mathrm{d}^2g_\nu/\mathrm{d}\nu^2$ can be obtained by solving the equations

$$(F^*F+\nu L)g_\nu=F^*h, \tag{13}$$

$$(F^*F+\nu L)\frac{\mathrm{d}g_\nu}{\mathrm{d}\nu}=-Lg_\nu, \tag{14}$$

$$(F^*F+\nu L)\frac{\mathrm{d}^2g_\nu}{\mathrm{d}\nu^2}=-2L\frac{\mathrm{d}g_\nu}{\mathrm{d}\nu}. \tag{15}$$

Numerically, to solve the linear matrix-vector Eqs. (13)–(15), we use the Cholesky (square root) decomposition method. A remarkable characteristic of the solution of Eqs. (13)–(15) is that the Cholesky decomposition of the coefficient matrix $F^*F+\nu L$ needs doing only once, then the three vectors g_ν, $\mathrm{d}g_\nu/\mathrm{d}\nu$, $\mathrm{d}^2g_\nu/\mathrm{d}\nu^2$ can be obtained readily. The algorithm is given in Appendix A.

4. NUMERICAL EXPERIMENTS

Numerically, the minimizer of the optimization problem (9) can be obtained by computing the gradient of the function

$$J^\nu[\mathbf{g}_t]:=\tfrac{1}{2}\|\mathcal{F}\mathbf{g}_t-\mathbf{h}_t\|^2+\nu/2\|L^{1/2}\mathbf{g}_t\|^2 \tag{16}$$

and setting the gradient to zero, where $\mathcal{F}$, $\mathbf{g}_t$, and $\mathbf{h}_t$ are all in discrete space corresponding to the continuous functions F, g, and h, respectively. Details about gradient computation of the function $J^\nu[\mathbf{g}_t]$ are given in Appendix B.

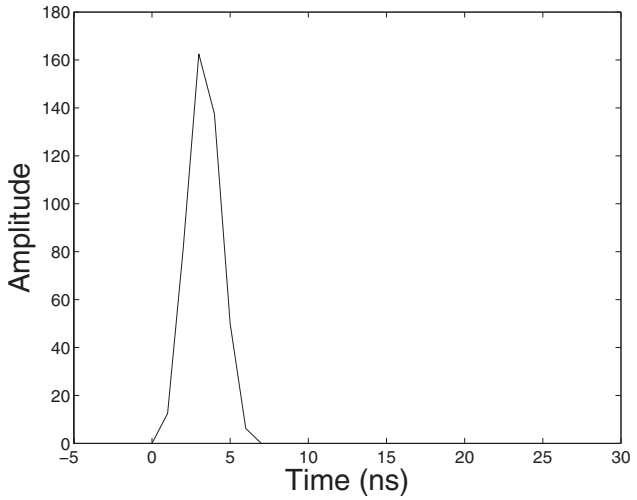

Fig. 1. Synthetic emitted laser pulse.

A. Synthetic Simulations

The analytical representation of the transmitted laser pulse and the true cross sections are given by third-order spline functions. For example, we generate the synthetic laser pulse function $f_{lp}(x)$ within the interval [2,3] by the formula

$$f_{lp}(x) = -31.25x^3 + 206.25x^2 - 356.25x + 218.75.$$

The synthetic laser pulse sampled with 1 ns resolution is shown in Fig. 1. The analytical representation of the cross section function $g_{cs}(x)$ within the interval $[3/8, 1/2]$ is given by the formula

$$g_{cs}(x) = 8x^3 - 10x^2 + 3x + 1/6.$$

The undistorted synthetic cross section is shown in Fig. 2.

The recorded waveform function $h_{wf}(x)$ (i.e., data) is calculated by a convolution of the splines representing the transmitted laser pulse ($f_{lp}(x)$) and the cross section ($g_{cs}(x)$) so that

$$h_{wf}(x) = f_{lp}(x) \star g_{cs}(x).$$

Note that h_{wf} represents the observation; this means different kinds of noise may be also recorded besides the true signal. Here we only consider a simple case: we assume that the noise is mainly additive Gaussian noise in [0,1], i.e.,

$$h_{wf} = h_{wf}^{true} + \delta\{\text{rand}[\text{size}(h_{wf}^{true})]\},$$

where $\delta > 0$ is the noise level, and rand[size(h_{wf}^{true})] is the Gaussian random noise with the same size as h_{wf}^{true}. In our simulation, the Gaussian random noise is generated with mean of zero and standard deviation of 2. The simulated waveform data with and without additional noise are plotted in Figs. 3–6, respectively.

We apply our regularization algorithm to recover the cross section and make a comparison. Initializations of implementing the regularizing algorithms are given in Appendix A. Comparisons of the true cross sections with the recovered cross sections are illustrated in Figs. 7 and 8 for noise levels of 1 and 2, respectively. It is apparent that our algorithm can find stable recoveries of the simulated synthetic cross sections. We do not list the plot of the comparison results for small noise levels since the algorithm yields perfect reconstructions.

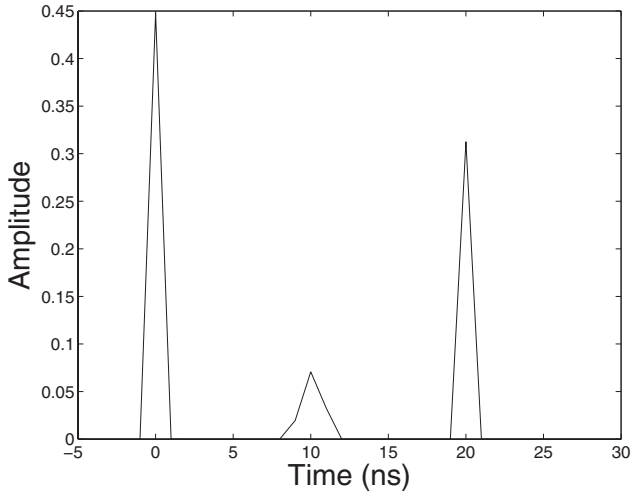

Fig. 2. Synthetic cross sections.

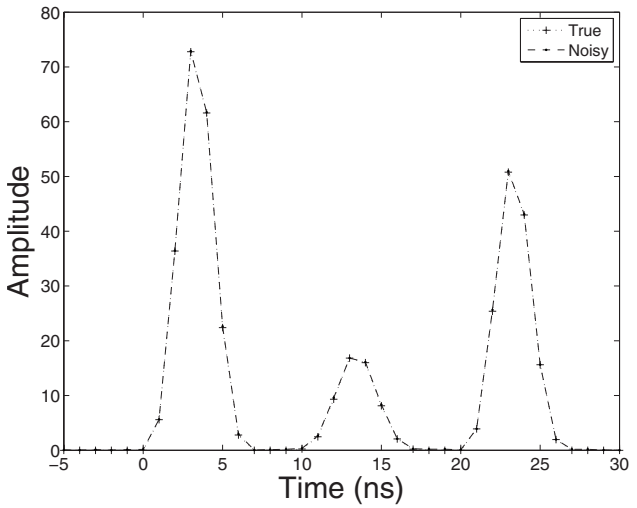

Fig. 3. Synthetic recorded waveform with and without addition of noise of level 1.

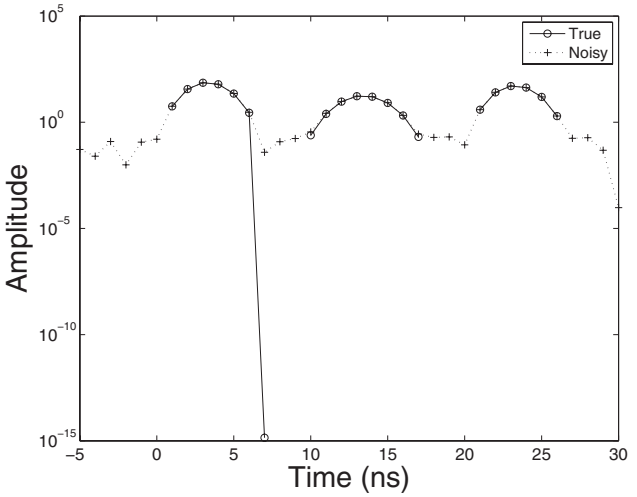

Fig. 4. Zoomed display of the synthetic recorded waveform with and without addition of noise of level 1.

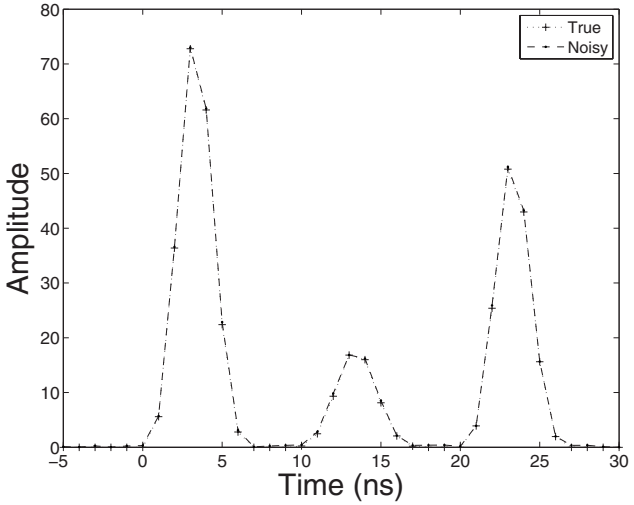

Fig. 5. Synthetic recorded waveform with and without addition of noise of level 2.

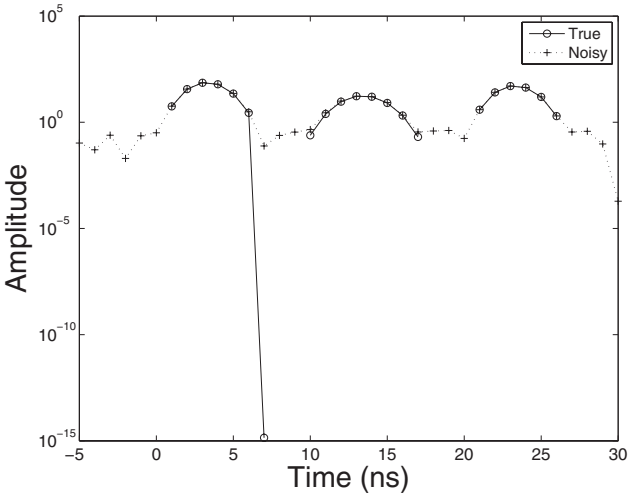

Fig. 6. Zoomed display of the synthetic recorded waveform with and without addition of noise of level 2.

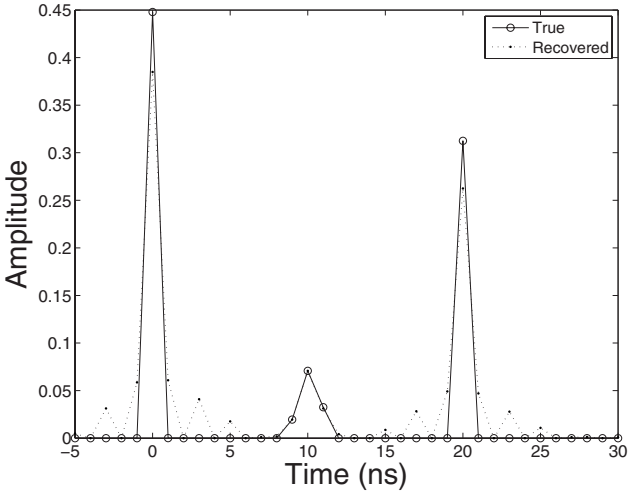

Fig. 7. Comparison of the true and recovered cross sections in the case of noise of level 1.

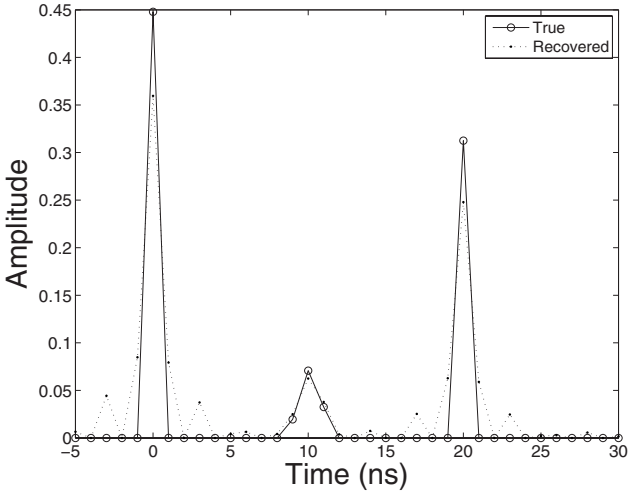

Fig. 8. Comparison of the true and recovered cross sections in the case of noise of level 2.

We also apply the traditional least-squares fitting method for computing the cross sections. However, the results are unsatisfactory. The correct cross section amplitude values cannot be well recovered. A comparison of results for a noise level of 2 is shown in Fig. 9.

To show the degree of fitness, we also evaluate the root mean-square error (rmse). Smaller rmse values indicate better precision of approximation. The rmse is defined by

$$\text{rmse} = \sqrt{\frac{1}{l}\frac{\sum_i [h_{comp}(x_i) - h_{meas}(x_i)]^2}{\sum_i [h_{comp}(x_i)]^2}}, \qquad (17)$$

which describes the average relative deviation of the retrieved signals from the true signals. Here h_{comp} refers to the retrieved waveform signals, h_{meas} refers to the measured unperturbed waveform signals, and l is the length of the vectors. The results are listed in Table 1. It reveals that for smaller noise levels, the degree of fitness of both methods is similar: while as noise levels increase, the rmse values of the least-squares fitting method increase

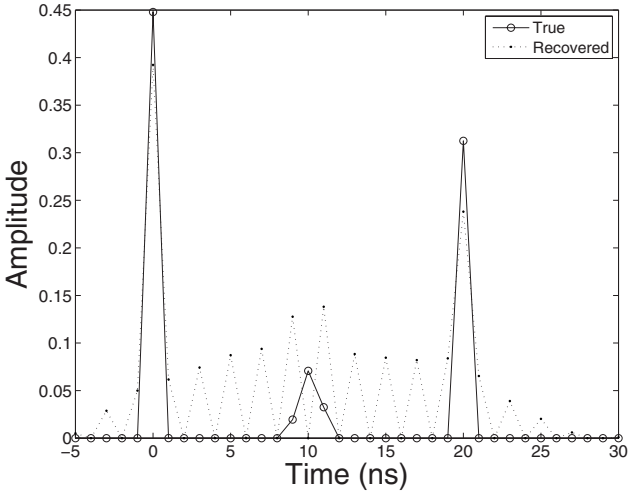

Fig. 9. Comparison of the true and recovered cross sections using least-squares fitting method in the case of noise of level 2.

Table 1. Comparison of RMSEs of Our Regularizing Algorithm with the Least-Squares Fitting Method for Different Noise Levels

Noise Level	Regularization Algorithm	LSE
0.01	8.9852e−4	4.8581e−4
0.05	8.4760e−3	2.4209e−3
0.1	1.5202e−2	4.8206e−3
0.5	2.6242e−2	2.3143e−2
1.0	3.1347e−2	4.3496e−2
2.0	3.3703e−2	7.6857e−2
3.0	3.4476e−2	9.9730e−2

rapidly, whereas the rmse values of the regularization algorithm increase slowly. This means that the regularization algorithm is more robust than the traditional least-squares fitting method.

B. Real Data Applications

Recently, three commercial airborne systems have become available, namely, the RIEGL LMS-Q560 (www.riegl.co.at), the TopEye Mark II system (www.topeye-.com), and Optech's ALTM 3100 system (www.optech.on.ca) (see [11]). The RIEGL LMS-Q560 became operational in 2004 (see [12]). The LMS-Q560 records all echo pulses (a copy of the transmitted laser pulse and the waveforms of its reflections). In this test, we use data from LMS-Q560. The ALS flight campaign was carried out in April 2007 in the Leithagebirge (Eastern Austria). The sample area contains open land as well as vegetation and buildings.

We tested the applicability of the proposed regularization method to LMS-Q560 data by performing a constrained optimizing fit to the measured waveforms. The illustrations of two samples of the emitted laser scanner sensor pulses are plotted in Figs. 10 and 14. As expected, the emitted laser pulse is close to a Gaussian function (relative differences $\leqslant 2\%$; see [3]). The recorded waveform of the first echo of this pulse is shown in Fig. 11 (dotted curve). We apply the algorithm presented in Subsection 3.D to compute the backscatter cross section. The result is shown in Fig. 12. The solid curve in Fig. 11 shows the reconstructed signal derived by the convolution of the emitted laser pulse and this cross section. One may see from Fig. 12 that there are several small oscillations outside the region $[4010, 4020]$ ns. But note that the amplitude of these oscillations is typically small; indeed, we consider they are noise or computational errors induced by noise when performing numerical inversion. However, they are controlled compared with the least-squares solution shown in Fig. 13, where noise propagation conceals the solution.

The return from the second emitted pulse (Fig. 14) consists of two scattering clusters in Fig. 15 (dotted curve). We applied our inversion algorithm again to retrieve the cross section (see Fig. 16 for the results). As in Fig. 11, the solid curve in Fig. 15 shows the reconstructed signal.

In both cases, the least-squares solution of this problem proved to be unstable, as already mentioned in Subsection 3.A. The respective results are therefore unsatisfactory, as shown in Figs. 13 and 17.

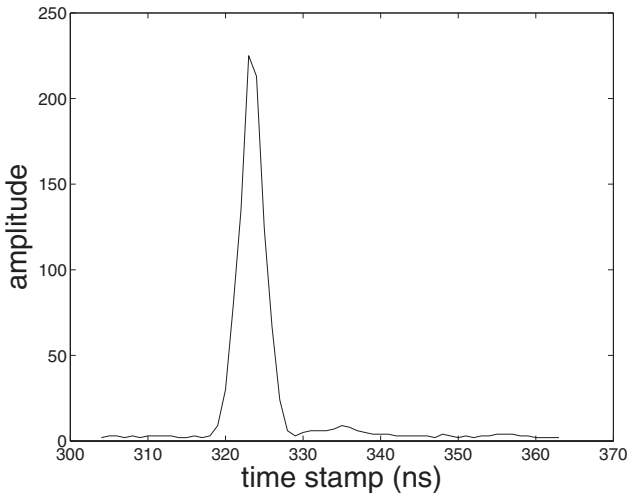

Fig. 10. First emitted laser pulse.

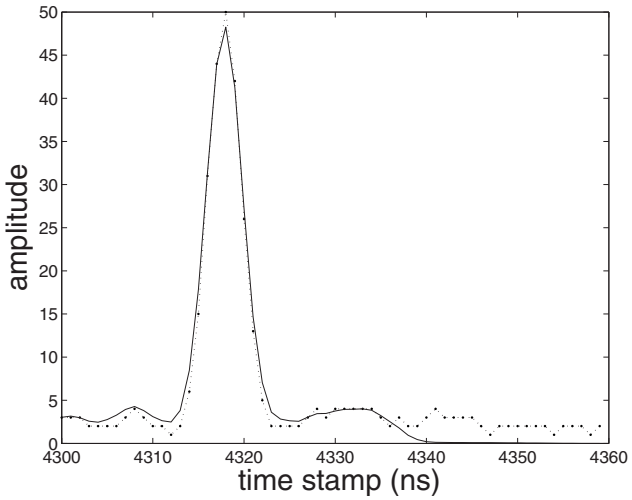

Fig. 11. Recorded echo waveform of the laser pulse shown in Fig. 10 (dotted curve) and its reconstruction using the cross section shown in Fig. 12 (solid curve).

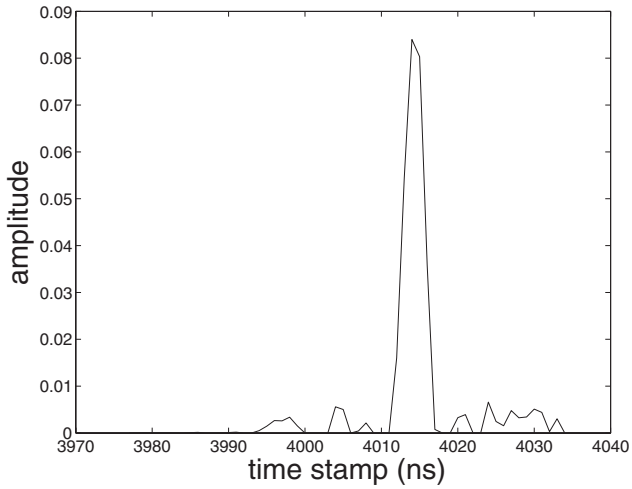

Fig. 12. Backscatter cross section in time domain of the waveforms in Figs. 10 and 11 calculated by regularized inversion.

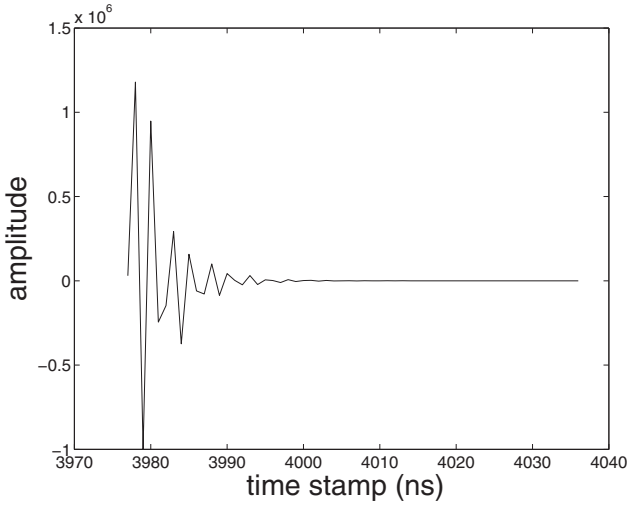

Fig. 13. Backscatter cross section in time domain of the waveforms in Figs. 10 and 11 calculated by least-squares fitting.

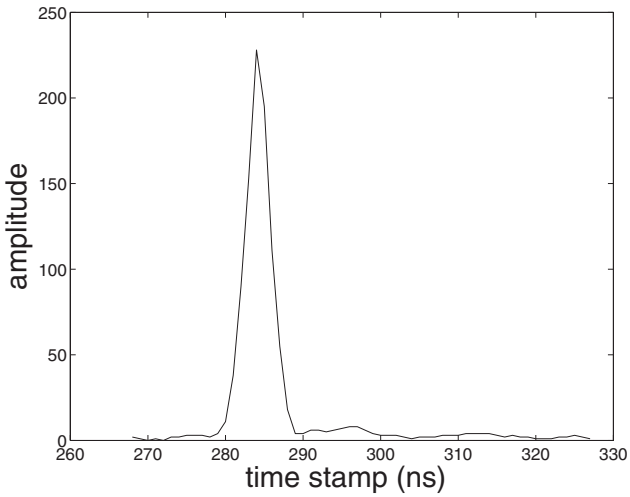

Fig. 14. Second emitted laser pulse.

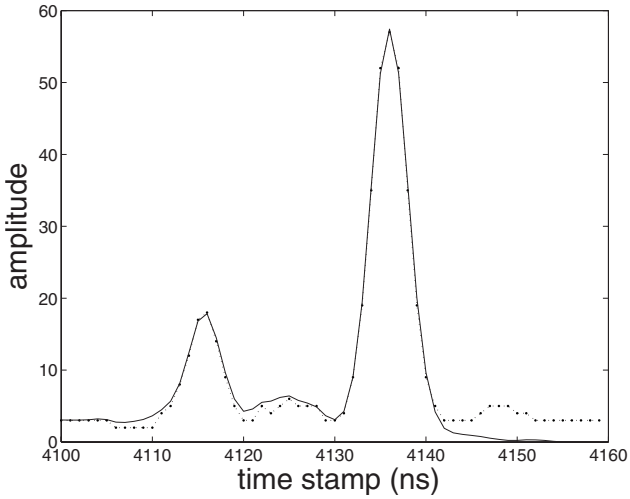

Fig. 15. Recorded echo waveform of the laser pulse shown in Fig. 14 (dotted curve) and its reconstruction using the cross section shown in Fig. 16 (solid curve).

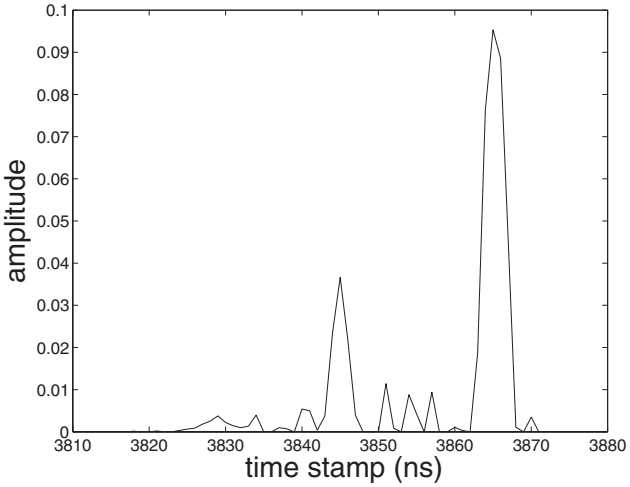

Fig. 16. Backscatter cross section in time domain of the waveforms in Figs. 14 and 15 calculated by regularized inversion.

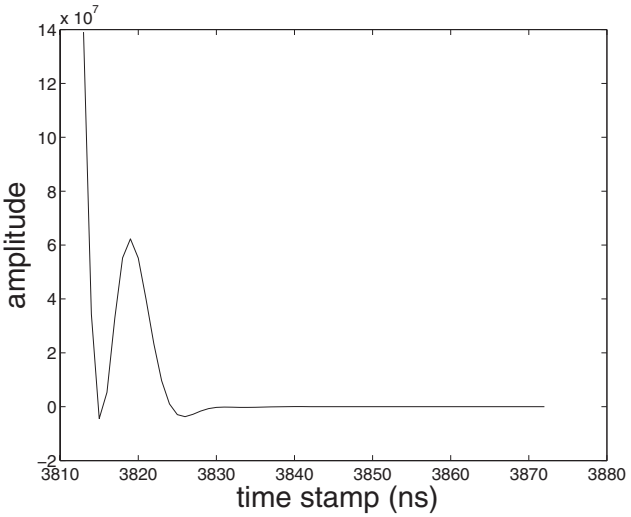

Fig. 17. Backscatter cross section in time domain of the waveforms in Figs. 14 and 15 calculated by least-squares fitting.

The inversion methods are quite important in practical applications. It is well understood that the land surface is quite complicated and in many cases it cannot be composed by pure Gaussian function combinations. Therefore the assumption about Gaussian decomposition of waveforms may be invalid sometimes. In addition, a major obstacle for determination of the scattering cross section from the observed waveform is the inherent ill-posed nature of the problem, i.e., we cannot hope to obtain a unique solution unless additional constraints based on *a priori* knowledge or assumptions are imposed. Tikhonov regularization is such a tool that can impose *a priori* knowledge readily. It utilizes both the stabilizer and the *a posteriori* parameter choice principle to control the stabilizer to seek a balance. As shown in our numerical examples, by utilizing the regularizing inversion method, we can always find reasonable cross sections. This shows the potential application of the proposed method.

5. CONCLUSION

The ill-posed nature of the model inversion is one of the most severe obstacles for a better estimation of the scat-

tering cross section of a land surface. Therefore it is desirable to develop new techniques for the robust estimation of the scattering cross section.

The regularization technique and its numerical treatment are developed in this paper and are proposed to retrieve laser scanner scattering cross section problems.

Our numerical simulations on synthetic data and real data show that the regularization method proposed in this paper is suitable for solving ill-posed laser scanner scattering cross section problems. However, we want to mention that the regularization algorithm relies on the proper regularization parameter and the balance between the noise level and the norm of the discrepancy [see Eq. (11)]. In some cases if the noise level cannot be estimated, new solution techniques should be considered. Since the regularization methods are based on the variational model, many optimization methods can be used to solve the problem. Interesting problems are how to construct efficient *a priori* information quantitatively and physically, how to terminate iterative algorithms to yield optimality and regularity, and how to use the retrieval results for the classification and segmentation of the interested region.

APPENDIX A: REGULARIZING ALGORITHM

In this appendix, we describe the procedure for choosing the regularization parameter by the method given in Subsection 3.D.

Algorithm A.1. (An *a posteriori* algorithm for solving the regularizing problem)

Step 1. Input $\mathcal{F}$, $\mathbf{h}_t$, L, the error level $\delta>0$, the initial guess value $\nu_0>0$, $k_{\max}$, and the stopping tolerance $\epsilon>0$; set $k:=0$;

Step 2. solve Eqs. (13)–(15);

Step 3. compute $\Psi(\nu_k)$, $\Psi'(\nu_k)$ and $\Psi''(\nu_k)$;

Step 4. update ν_{k+1} by iterative formula (12);

Step 5. if $|\nu_{k+1}-\nu_k|\leqslant\epsilon$ or $k=k_{\max}$, STOP; otherwise, set $k:=k+1$, GOTO Step 2.

In our numerical tests, the parameters are $\nu_0=0.1$, $\epsilon=1.0e-6$, and $k_{\max}=400$. For our synthetic simulations, the noise levels are known, so they can be used directly in the algorithm. For real data applications, the noise level has to be estimated. We believe our data are of good quality, so a smaller noise level $\delta=1.0e-4$ was used. For solving Eqs. (13)–(15), we use the Cholesky decomposition method, i.e., we first decompose $\mathcal{F}^T\mathcal{F}+\nu L=G^TG$, and then solve $G^TG\mathbf{g}_t=\mathbf{y}$ by $G^T\mathbf{u}=\mathbf{y}$, $G\mathbf{g}_t=\mathbf{u}$, where $\mathbf{y}=\mathcal{F}^T\mathbf{h}_t$.

APPENDIX B: GRADIENT COMPUTATION

In the following, we assume the norm $\|\cdot\|$ belongs to the discrete l_2 space. Numerically, the minimizer of the optimization problem (9) can be obtained by computing the gradient of the functional

$$J^\nu[\mathbf{g}_t]:=\tfrac{1}{2}\|\mathcal{F}\mathbf{g}_t-\mathbf{h}_t\|^2+\nu/2\|L^{1/2}\mathbf{g}_t\|^2. \tag{B1}$$

For any ϕ in the definition domain of $\mathcal{F}$ and $\rho\in\mathbb{R}$, we have

$$\begin{aligned}J^\nu[\mathbf{g}_t+\rho\phi]=&\,1/2(\|\mathcal{F}\mathbf{g}_t-\mathbf{h}_t\|^2+\nu\|L^{1/2}\mathbf{g}_t\|^2\\&+\rho/2[(\mathcal{F}\mathbf{g}_t-\mathbf{h}_t,\mathcal{F}\phi)+(\mathcal{F}\phi,\mathcal{F}\mathbf{g}_t-\mathbf{h}_t)\\&+\nu(L^{1/2}\mathbf{g}_t,L^{1/2}\phi)+\nu(L^{1/2}\phi,L^{1/2}\mathbf{g}_t)]\\&+\rho^2/2(\|\mathcal{F}\phi\|+\nu\|L^{1/2}\phi\|^2).\end{aligned}$$

Hence,

$$\begin{aligned}&\frac{\mathrm{d}}{\mathrm{d}\rho}J^\nu[\mathbf{f}_t+\rho\phi]\big|_{\rho=0}\\&\quad=(\mathcal{F}\mathbf{g}_t-\mathbf{h}_t,\mathcal{F}\phi)+\nu(L\mathbf{g}_t,\phi)=[(\mathcal{F}^T\mathcal{F}+\nu L)x-\mathcal{F}^T\mathbf{h}_t,\phi],\end{aligned}$$

which yields the gradient given by

$$\mathrm{grad}_{\mathbf{g}_t}\{J^\nu[\mathbf{g}_t]\}=(\mathcal{F}^T\mathcal{F}+\nu L)\mathbf{g}_t-\mathcal{F}^T\mathbf{h}_t.$$

By the first-order necessary condition (see, e.g., [13]), the minimizer $\mathbf{g}_t^\nu$ should satisfy $\mathrm{grad}_{\mathbf{g}_t}[J^\nu[\mathbf{g}_t^\nu]]=0$, which leads to solving the nonhomogeneous linear system

$$\mathbf{g}_t=(\mathcal{F}^T\mathcal{F}+\nu L)^{-1}\mathcal{F}^T\mathbf{h}_t. \tag{B2}$$

This is a well-posed system, hence, standard linear algebraic methods can be used.

ACKNOWLEDGMENTS

We thank the referees for valuable suggestions which greatly helped us improve the quality of the paper. The first author gives special thanks to I.P.F in Wien for supporting his visit in November 2007. This research is supported by National "973" Key Basic Research Developments Program of China under grants 2005CB422104 and 2007CB714400 and National Natural Science Foundation of China (NSFC) under grant 10871191.

REFERENCES

1. H. C. Chang, L. L. Ge, C. Rizos, and T. Milne, "Validation of DEMs derived from radar interferometry, airborne laser scanning, and photogrammetry by using GPS-RTK," in *Proceedings of 2004 IEEE International Geoscience and Remote Sensing Symposium* (IEEE, 2004), Vol. 5, pp. 2815–2818.
2. M. Flood, "Laser altimetry: from science to commercial lidar mapping," Photogramm. Eng. Remote Sens. **67**, 1209–1217 (2001).
3. W. Wagner, A. Ullrich, V. Ducic, T. Melzer, and N. Studnicka, "Gaussian decomposition and calibration of a novel small-footprint full-waveform digitising airborne laser scanner," ISPRS J. Photogramm. Remote Sens. **60**, 100–112 (2006).
4. W. Wagner, A. Ullrich, T. Melzer, C. Briese, and K. Kraus, "From single-pulse to full-waveform airborne laser scanners: potential and practical challenges," Int. Arch. Photogramm. Remote Sens. Spat. Inf. Sci. **35**, 201–206 (2004).
5. Y. F. Wang, X. W. Li, Z. Nashed, F. Zhao, H. Yang, Y. N. Guan, and H. Zhang, "Regularized kernel-based BRDF model inversion method for ill-posed land surface parameter retrieval," Remote Sens. Environ. **111**, 36–50 (2007).
6. Y. F. Wang, C. C. Yang, and X. W. Li, "A regularizing kernel-based BRDF model inversion method for ill-posed land surface parameter retrieval using smoothness constraint," J. Geophys. Res. **113**, D13101 (2008).
7. A. N. Tikhonov and V. Y. Arsenin, *Solutions of Ill-Posed Problems* (Wiley, 1977).

8. M. Z. Nashed, "Perturbations and approximations for generalized inverses and linear operator equations," in *Generalized Inverses and Applications* M. Z. Nashed, ed. (Academic, 1976), pp. 325–396.
9. Y. F. Wang, S. F. Fan, X. Feng, G. J. Yan, and Y. N. Guan, "Regularized inversion method for retrieval of aerosol particle size distribution function in $W^{1,2}$ space," Appl. Opt. **45**, 7456–7467 (2006).
10. Y. F. Wang and T. Y. Xiao, "Fast realization algorithms for determining regularization parameters in linear inverse problems," Inverse Probl. **17**, 281–291 (2001).
11. Å. Persson, U. Söderman, J. Töpel, and S. Ahlberg, "Visualization and analysis of full-waveform airborne laser scanner data," Int. Arch. Photogramm. Remote Sens. Spat. Inf. Sci. **36**, 103–108 (2005).
12. C. Hug, A. Ullrich, and A. Grimm, "LITEMAPPER-5600-a waveform digitising lidar terrain and vegetation mapping system," Int. Arch. Photogramm. Remote Sens. Spat. Inf. Sci. **36**, 24–29 (2004).
13. Y. F. Wang, *Computational Methods for Inverse Problems and Their Applications* (Higher Educational Press, Beijing, 2007).